Journal of Molecular Liquids 204 (2015) 50–59

Contents lists available at ScienceDirect

Journal of Molecular Liquids

journal homepage: www.elsevier.com/locate/molliq

A magnetic fluid based on covalent-bonded nanoparticle organic hybrid materials (NOHMs) and its decolorization application in water

Kun-Yi Andrew Lin [a,*], Hongta Yang [b], Wei-Der Lee [a], Kuan-Yi Tsao [b]

[a] Department of Environmental Engineering, National Chung Hsing University, Taichung, Taiwan, ROC
[b] Department of Chemical Engineering, National Chung Hsing University, 250 Kuo-Kuang Road, Taichung, Taiwan, ROC

ARTICLE INFO

Article history:
Received 29 October 2014
Received in revised form 30 December 2014
Accepted 13 January 2015
Available online 15 January 2015

Keywords:
Nanoparticle organic hybrid materials
Magnetic fluid
Decolorization

ABSTRACT

Nanoscale organic hybrid materials (NOHMs) are surface-functionalized nanoparticles which can exhibit liquid-like behavior without addition of solvents. NOHMs can be prepared via grafting polymer chains to the surface of nanoparticle by ionic bonding or covalent bonding. While the ionic-bonded NOHMs have been investigated extensively, studies and applications of the covalent-bonded NOHMs are still limited. This study aims to examine the applicability of the covalent-bonded NOHMs in aqueous solutions. To facilitate separation of the covalent-bonded NOHMs from water, we developed this magnetic NOHMs fluid (MNF) and used it to decolorize dyes in water. This MNF was synthesized using γ-Fe_2O_3 as a core and polyetheramine as polymer chains. The as-synthesized MNF was characterized by SQUID, TEM, FT-IR, XRD, rheometer and thermogravimetric analyzer. The decolorization of dye in water using MNF was demonstrated by removing Nile Blue dye from water. The dye removal capacity of MNF as a function of time was measured and analyzed using the pseudo first and second order rate laws as well as the intra-particle diffusion. In addition, the Langmuir isotherm appeared to satisfactorily represent the sorption isotherm data. The fluid and magnetically responsive MNF showed its potential applicability in aqueous solutions to expand the functionality and applications of covalent-bonded NOHMs.

1. Introduction

Advancement of functional nanoparticles has been fueled by linking various functional molecules to the surface of the nanoparticles to exhibit miscellaneous properties. In particular, with coating of special polymers, surface-functionalized nanoparticles have been developed to display unique liquid behaviors without any solvents [1,2]. This type of liquid-like functionalized nanoparticles is named as "nanoparticle organic hybrid materials (NOHMs)" [3–6]. Liquid-like NOHMs can be synthesized by grafting polymer chains via ionic bonding or covalent bonding to nanoparticles [3]. Therefore, NOHMs can reveal several advantages compared to traditional colloidal suspensions [7]. First, the grafted polymers are chemically bonded to the nanoparticles in NOHMs while the liquid medium and the nanoparticle are just physically discrete components in the traditional colloidal suspension [1,2,7]. As a result, NOHMs display distinct thermodynamic properties from the traditional colloidal suspension. Furthermore, a unit of NOHMs consists of a nanoscale core and polymer chains. These two components can be selectively designed to obtain specific functionality toward a given application [3,8]. Additionally, since the polymer chains are bonded to the nanoparticles in NOHMs, the loss of the polymer chains can be prevented, thereby reducing their vapor pressure. Thus, NOHMs are considered as a new class of polymeric nanocomposites [8] and polymeric colloids [9].

Recently, the ionic-bonded NOHMs have been assigned with the specific name "nanoscale ionic materials (NIMs)" [7,8,10] which have been extensively investigated and developed using various types of "nanoscale cores", including SiO_2 [1,2,4–8,11–13], γ-Fe_2O_3 [2,14], DNA [1], ZnO [15], carbon nanotubes [16], and graphene [10]. NIMs can behave as liquids and their unique ionic bonding enables the polymer to be tightly anchored to the nanoscale cores. Consequently, NIMs have drawn a great deal of attention and have been proposed for numerous applications such as lubricants [17], electrolytes [18,19], CO_2 capture solvents [3], and SO_2 capture solvents [20].

On the other hand, studies reporting applications of covalent-bonded NOHMs are still limited to gas phase applications [21]. However, the covalent-bonded NOHMs could be more advantageous than the ionic bonded NOHMs in certain applications considering that the polymer chains are tethered covalently to the nanoparticles. Since the covalent bonding is less likely to dissociate in aqueous medium, the covalent-bonded NOHMs can be used for applications involving aqueous solutions, such as wastewater treatment, water purification and liquid–liquid extraction. Especially in the wastewater treatment and water purification, the contaminated wastewater may contain various salts, acids, bases and charged surfactants which can interfere (or even react with) the ionic bonding of the ionic-bonded NOHMs and impart the

* Corresponding author at: Department of Environmental Engineering, National Chung-Hsing University, Taichung, Taiwan, ROC.
E-mail address: linky@nchu.edu.tw (K.-Y.A. Lin).

http://dx.doi.org/10.1016/j.molliq.2015.01.020
0167-7322/

structure of NOHMs. Thus, the covalent-bonded NOHMs appear to be more suitable to be used in the aqueous applications compared to the ionic-bonded one.

Given that the covalent-bonded NOHMs have only been considered in gas absorption applications, it is interesting and necessary to examine their applicability in aqueous medium. Therefore, in the present study, we developed a covalent-bonded NOHM and examined its capability of dye-decolorization in water. Many materials have been used to decolorize dyes in water, such as carbonaceous materials [22–24], mesoporous sorbents [25,26], and ion exchange resins [27]. However, these materials were solid and most of them have to be stirred in order to suspend in aqueous solutions and to increase the contact between adsorbates and adsorbents. Since NOHMs behave like liquids which can "dissolve" in the solutions, NOHMs are expected to be well-suspended in the solutions without vigorous stirring. Additionally, when the solid materials are used in the aqueous applications, most of the contact between the solid materials and adsorbates occurs on the surface of the solid materials. However, each polymer chain of NOHMs is tethered to the nanoparticles only with one end and the polymer chain can still fully expose itself to the adsorbates to increase the contact. Therefore, NOHMs can be a useful alternative material for the aqueous application, namely the decolorization.

Since NOHMs can be "dissolved" in water, it is necessary to separate them from water after the decolorization. Therefore, the covalent-bonded NOHMs must possess responsiveness upon external driving forces for the separation from water. To this end, we embedded magnetic responsiveness with the covalent-bonded NOHM and enabled it re-collectable in water using the external magnet field. The resulting magnetic liquid-like covalent-bonded NOHM was called the magnetic NOHMs fluid (MNF). This MNF can be distinguished from conventional magnetic fluids: conventional magnetic fluids are prepared by mixing only magnetic iron oxide nanoparticles (IONs) and solvents [28–31] whereas IONs and the polymer chains in MNF are chemically bonded. Therefore, when MNF is dissolved in water, the entire unit of MNF (i.e., both polymer chains and IONs) can be drawn by an external magnetic field to recover the IONs and the polymer. In this study, we synthesized MNF via grafting polyetheramine to γ-Fe_2O_3 IONs. MNF was characterized using SQUID to determine its saturation magnetization whereas TEM was used to examine its microscopic morphology and the size distribution of IONs in MNF. To investigate MNF's chemical composition, FT-IR and XRD were employed. Additionally, since MNF is a liquid material, its rheological property was measured and compared to its precursor, polyetheramine. The thermal stability of MNF and its precursor materials were also tested to reveal its enhanced thermal stability. The decolorization using MNF was demonstrated by removing Nile Blue dye from aqueous solutions. To investigate the decolorization behavior, the dye-removal kinetics was examined using the pseudo first rate law, the pseudo second order rate law as well as the intra-particle diffusion model. The sorption isotherms, including the Langmuir, Freundlich, Temkin and Dubinin–Rudashkevich (D–R) models, were also used to analyze the decolorization data to provide insights into the decolorization mechanism.

2. Experimental

2.1. Materials

The commercially available chemicals involved in the study were used as received without additional purification. Iron sulfate $Fe(SO_4)\cdot 7H_2O$ was purchased from Merck (Germany), (3-glycidyloxypropyl) trimethoxysilane from Gelest Inc. (USA), ammonium hydroxide from Showa Chemicals (Japan), and Nile Blue A from Alfa Aesar (USA). Polyetheramine (Jeffamine M2070, density = 1.07 g cm^{-1}) was a gift kindly provided by Taiwan Huntsman (Taiwan). Acid Red 27 dye, Acid Yellow 17 dye, and oleic acid were obtained from Sigma-Aldrich (USA). Methylene blue dye and malachite green dye were obtained from Choneye Pure Chemicals (Taiwan). Cellulose dialysis membrane (MWCO: 6000–8000 Da) was purchased from Cellu·Sep (USA). Deionized (D.I.) water was prepared to exhibit less than 18.0 MΩ cm.

2.2. Synthesis of magnetic NOHMs fluid

A single unit of MNF essentially consists of a single ION and polymer chains which attach to the surface of the ION. The γ-Fe_2O_3 IONs were prepared according to reported procedures [14,21]. Firstly, 5 g of $Fe(SO_4)\cdot 7H_2O$ was dissolved in 60 ml of D.I. water, followed by addition of 7 ml of ammonium hydroxide (28%) and then 0.5 ml of H_2O_2 (30%) to form Part I solution. Next, 8 ml of oleic acid, as a surfactant, was dissolved in 100 ml of toluene to form Part II solution. While the Part I solution was stirred, the Part II solution was slowly added to the Part I solution. The resultant mixture was then heated to 95 °C and stirred for 45 min. In the end of the reaction, 50 ml of acetone was poured to the mixture and the dark-color precipitate was collected, washed by acetone repeatedly and dried at 70 °C to yield the IONs.

The polymer chain was synthesized by reacting polyetheramine with (3-glycidyloxypropyl)trimethoxysilane to form a polyetheramine–silane [21] as shown in Fig. 1(a). In a typical preparation, 5 g of polyetheramine was added to 200 ml of ethanol and the solution was stirred and heated at 70 °C. Next, 1 g of (3-glycidyloxypropyl)trimethoxysilane was dropwise added to the solution which then was stirred and maintained at 70 °C for 12 h to obtain the polyetheramine–silane. To graft the polyetheramine–silane to the IONs (Fig. 1(b)), the as-synthesized IONs were firstly added to 100 ml of ethanol and sonicated for 30 m to disperse IONs in ethanol. The suspension of IONs then was slowly poured to the polyetheramine–silane solution while stirring. The mixture of IONs and polyetheramine–silane was stirred vigorously and kept at 70 °C for 24 h to silanize the IONs with the polyetheramine–silane. Once the reaction was finished, the dialysis membrane was used to dialyze the colloidal suspension against D.I. water for 24 h to remove unreacted compounds. Finally, the dialyzed product was dried under reduced pressure at 70 °C to remove water to yield a dark color fluid, MNF.

2.3. Characterization of magnetic NOHMs fluid

To observe the response of MNF under an external magnetic field, a 1.5-ml glass vial containing 0.5 ml of MNF was placed next to a permanent neodymium magnet. The movement of MNF was monitored using a digital camera (Canon SX500IS). Magnetization of MNF was measured by a Superconducting Quantum Interference Device (SQUID) Vibrating Sample Magnetometer (Quantum Design MPMS SQUID VSM, USA) at 27 °C. The microscopic morphology of MNF was obtained using a Transmission Electronic Microscopy (JEOL JEM-2010, Japan). Fourier-transform infrared (IR) spectroscopic analyses of MNF and its precursor materials were conducted using an infrared spectrometer (4100, Jasco, Japan). The X-ray diffraction patterns (XRD) of MNF and the IONs were characterized using an X-ray diffractometer (PANalytical, the Netherlands) with copper as an anode material (40 mA, 45 kV). The rheological behaviors of MNF and its precursor, polyetheramine, were measured using a stress-controlled rheometer (Anton Parr MCR101, Austria) equipped with a 25-mm parallel plate at 27 °C. To investigate the thermal stabilities of MNF and its precursor materials, the weight loss as a function of temperature was measured by a thermogravmetric analyzer (TGA) (ISI 1000, USA) with a carrier gas of nitrogen.

2.4. Decolorization of dye-containing water using MNF

Decolorization capability of MNF was demonstrated by removing Nile Blue dye from water. Nile Blue dye was selected as the model dye because it is soluble in water and can be found in wastewater [32]. The chemical structure of Nile Blue dye can be also seen in Fig. S1 (see ESI†). In a typical decolorization experiment, 0.1 g of MNF was added to a 20-ml glass vial and then 5 ml of D.I. water was poured into the

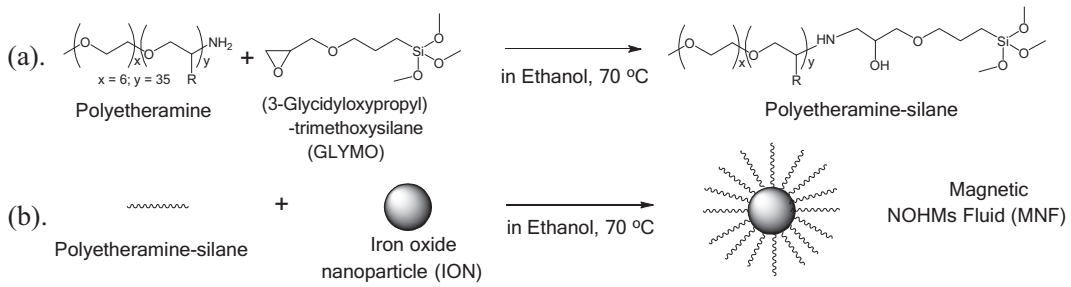

Fig. 1. Scheme of synthesis of magnetic NOHMs fluid (MNF): (a) preparation of polyetheramine–silane and (b) synthesis of MNF by silanizing iron oxide nanoparticles (IONs) with polyetheramine–silane.

glass vial to disperse MNF to form a MNF solution. Next, 15 ml of aqueous solution of Nile Blue dye of a pre-set concentration was added to the MNF solution to reach a desired concentration (i.e., 40–160 mg l^{-1}) of Nile Blue dye. The mixture immediately was placed on the temperature-controllable orbital shaker (Yih-Der, Taiwan) at 300 rpm at 25 °C for a certain mixing time, t. To evaluate the decolorization efficiency (removal capacity), MNF and the aqueous solution were separated first using the external magnet to collect the supernatant which was further filtered by 0.22 μm PVDF membrane filter to ensure the complete removal of MNF from the aqueous solution. The filtrate was then analyzed using a UV–VIS spectrophotometer (Chrom-Tech CT-2000, Taiwan) to determine the amount of Nile Blue dye remained in the solution at a wavenumber of 550 cm^{-1}.

The removal capacity, q_t (mg g^{-1}) of MNF after a mixing time, t (min), was calculated by $q_t = V(C_0 - C_t)/m$ where V (l) is the total volume of the mixture, C_0 (mg L^{-1}) the initial concentration of Nile Blue dye in water, C_t (mg L^{-1}) the remaining concentration of Nile Blue dye in water after a mixing time t, and m (g) the weight of MNF added in the glass vial.

3. Results and discussion

3.1. Characterizations of magnetic NOHMs fluid

3.1.1. Response under an external magnet and magnetization

The as-synthesize MNF was filled in a glass vial as shown in Fig. 2(a). Although MNF consisted of a high fraction of polymer chains (~95 wt.%) which are transparent, MNF exhibited a dark brownish color derived from γ-Fe_2O_3 nanoparticles. It also can be seen that the color of MNF was homogenous and no phase separation was observed. This suggests that the IONs were stably and evenly "suspended" inside the polymeric medium (i.e., polyetheramine). To compare with MNF, IONs were physically mixed with polyetheramine to investigate the distribution of IONs in polyetheramine when two components were just blended. Fig. S2(a) (see ESI†) displays a glass vial filled with the transparent polyetheramine, to which dark-color IONs were added as shown in Fig. S2(b). One can quickly observe the settling of IONs inside the glass vial due to the much higher density of IONs (4.9 g cm^{-3}) [33] than that of polyetheramine (1.07 g cm^{-3}). After the mixture was stirred and left on the bench for 5 min, the IONs still settled to the bottom of the vial and the phase separation occurred (Fig. S2(c)). This comparison revealed that MNF exhibited a unique colloidal system in which nanoparticles were stably suspended and no phase separation occurred [1,2,8,12].

Fig. 2(a) also shows that the surface of MNF was noticeably raised inside the glass vial. This raised surface might derive from the capillary effect, suggesting that small contact angle could exist between MNF and the glass wall because of the hydrophilicity of polyetheramine [34]. Once the glass vial approached a permanent magnet (Fig. 2(b)), the surface level of MNF significantly leaned toward the center of the magnet where the strongest magnetic field is located. The feature demonstrated that MNF behaved as a liquid and readily responsive to the external magnetic field. To quantitatively determine the magnetization of MNF, SQUID analysis was performed and the result is shown in Fig. 2(c). It can be seen that at the ambient temperature, MNF can exhibit a saturation magnetization of 1.05 A m^2 kg^{-1}. Because the IONs only accounted for ~5 wt.% of the total mass of MNF, this value is relatively low compared to the typical saturation magnetization of γ-Fe_2O_3 (i.e., 30 A m^2 kg^{-1}) [35]. However, saturation magnetization of MNF was comparable to that of the conventional magnetic fluids [28]. The magnetically controllable capability of MNF can be further improved by increasing γ-Fe_2O_3 fraction in MNF as well as the strength of magnetic field.

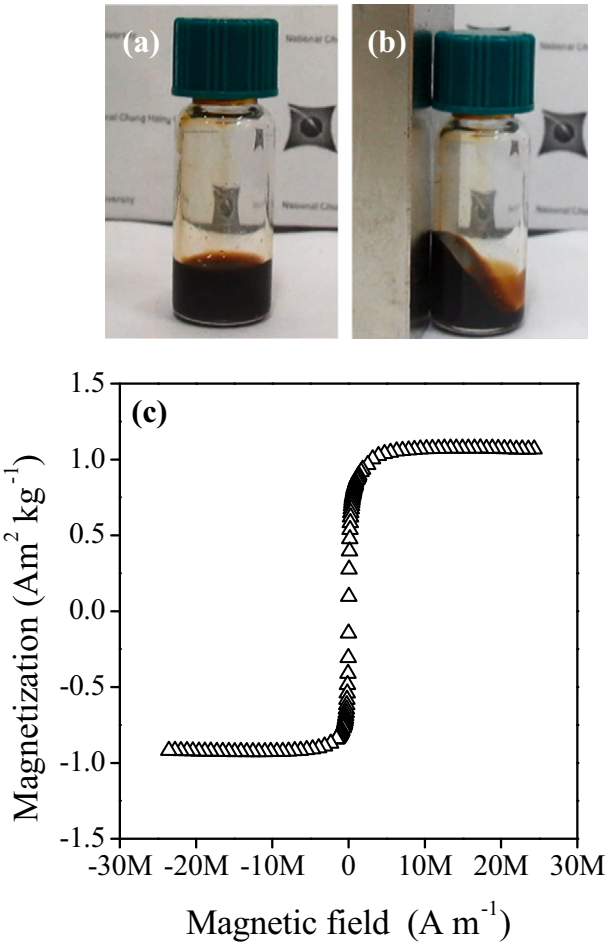

Fig. 2. Pictures showing (a) bulk MNF and (b) its response under a magnetic field as well as (c) magnetization of MNF at the ambient temperature.

3.1.2. Chemical composition analysis and morphology of MNF

The chemical composition of MNF was analyzed using the FT-IR spectroscopy. Fig. 3(a) shows spectra of MNF and its precursor materials including (3-glycidyloxypropyl)-trimethoxysilane, polyetheramine, and polyetheramine–silane. It can be seen that the spectrum of polyetheramine–silane was similar to that of polyetheramine. However, the signature peak of (3-glycidyloxypropyl)trimethoxysilane at 3056 cm^{-1} (ν_{C-H} epoxy) was not observed in the spectrum of polyetheramine–silane, suggesting that epoxy groups of (3-glycidyloxypropyl)trimethoxysilane had reacted with the primary amine group of polyetheramine and the epoxy ring opened [21]. The IR spectrum of MNF was also similar to that of polyetheramine–silane which displayed two major signature peaks at 1120 and 2883 cm^{-1} derived from C–O and C–H groups of polyetheramine, respectively. Crystalline structures of MNF and its precursor materials can be seen from their XRD patterns in Fig. 3(b). The peaks of IONs at 30.2°, 36.52°, 43.52°, 53.54° and 62.64° can be readily indexed to (2 2 0), (3 1 1), (4 0 0) and (4 4 0) crystal planes of γ-Fe_2O_3 (JCPDS 39-1346). When IONs were silanized with the polyetheramine–silane to form MNF, the same features can be observed in the pattern of MNF in which the peaks at 30.2°, 36.52°, 43.52° and 62.64° can be visibly identified, indicating that the IONs in MNF remained as γ-Fe_2O_3.

To investigate the microscopic morphology of MNF, a TEM image of MNF was taken and shown in Fig. 4(a). The image displays the distribution of IONs (i.e., dark-color particles) in the organic polyetheramine medium (i.e., the light-color region). One can observe that these IONs were nano-scale and most of nanoparticles were mono-dispersed without aggregation. This morphology was significantly different from the morphology of pristine IONs (Fig. S3, see ESI†), in which the IONs were closely packed because no polymeric medium existed on the exterior of the ION. In contrast, the surface of IONs was functionalized with polyetheramine–silane in MNF, thereby preventing IONs from the aggregation [3,8].

To analyze the size distribution of IONs in MNF, diameter of each particle was determined and summarized as a histogram plot shown in Fig. 4(b). The size distribution was fitted by a Gaussian distribution with a mean of 12.36 nm, a standard deviation of 8.67 nm and a correlation coefficient (R^2) of 0.955.

3.1.3. Physical properties of magnetic NOHMs fluid

As a liquid material, it is important to investigate the rheological behavior of MNF and compare with its precursor, polyetheramine. Fig. 5(a) shows the storage modulus (G′), the loss modulus (G″), and the complex viscosity ($^*\eta$) of MNF and polyetheramine. For polyetheramine, G′ was noticeably lower than G″ in the range of applied strain from 0 to 1000%. This indicates that the rheological behavior of polyetheramine, without the introduction of IONs, was mainly subject to the viscous behavior. It also can be seen that when the relatively low strain was applied on polyetheramine, a short stable region was observed, indicating the existence of linear viscoelasticity in polyetheramine. Additionally, G″ of polyetheramine remained constant throughout the range of applied strain. When IONs were functionalized with polyetheramine–silane to form MNF, G′ of MNF was found to be similar that of polyetheramine. However, the stable region G′ of MNF was much shorter than that of polyetheramine. G′ of MNF also gradually decreased after the stable region rather than exhibiting a distinct yield point as polyetheramine. This suggests that the viscoelasticity of polyetheramine has been modified after the introduction of IONs to form MNF. On the other hand, G″ of MNF was also significantly higher than its G′, showing that the rheological behavior of MNF was still subject to the viscous behavior. Interestingly, G″ of MNF was noticeably higher than that of polyetheramine by almost an order of magnitude. Such a difference reveals that the rheology of MNF became more dominant by its viscous behavior due to the presence of IONs. This feature was also reflected on the complex viscosity ($^*\eta$) of MNF which was found to be 0.140 Pa s, much higher than that of polyetheramine, 0.025 Pa s. While the existence of IONs in MNF led to noticeable changes in the rheological behavior, MNF was still able to behave as a free-flow liquid.

With the introduction of IONs in polyetheramine to form MNF, it is also expected that the bonding and the physical contact between polyetheramine and IONs can enable MNF to exhibit a higher thermal stability than polyetheramine [3]. Fig. 5(b) displays the thermal stabilities of MNF and its precursor materials. To quantitatively analyze the thermal stability, a temperature at which 50% weight loss of each material occurred was denoted as T_{50} [36] and used to compare thermal stabilities of different materials. It can be seen that T_{50} for (3-glycidyloxypropyl)-trimethoxysilane was 172 °C, whereas T_{50} for polyetheramine was found to be 212 °C. After polyetheramine reacted with (3-glycidyloxypropyl)trimethoxysilane to form polyetheramine–silane, T_{50} was shifted considerably to 277 °C, showing a significant improvement in thermal stability. When polyetheramine–silane was grafted to the surface of IONs to form MNF, T_{50} was further advanced to 329 °C. This remarkable increase in T_{50} in MNF revealed that the introduction of IONs contributed greatly to enhance thermal stability. Since polyetheramine–silane was grafted to IONs by forming a covalent-bonded silica network on the surface of IONs, such a covalent bonding effectively anchored polyetheramine polymer chains to IONs [37]. Therefore polyetheramine polymer chains can stand up to a higher temperature. Additionally, the physical contact between IONs and polyetheramine may also contribute to the enhancement of thermal stability [38–49]. On the other hand, the residual mass of MNF after

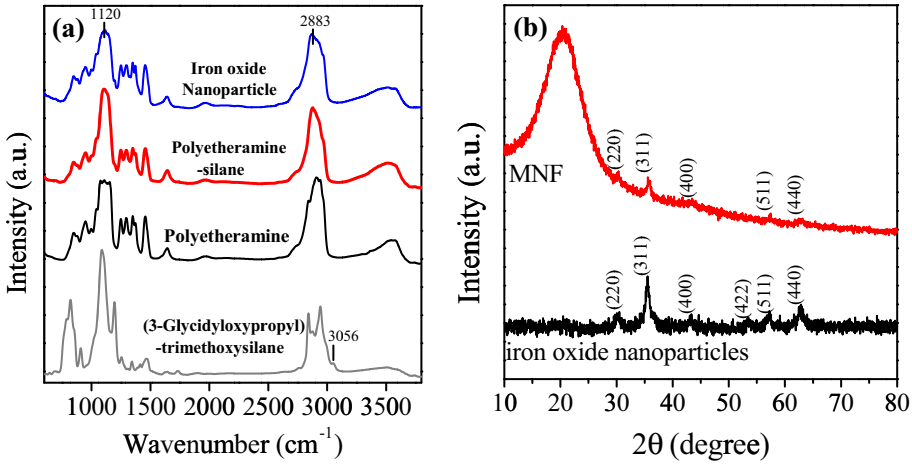

Fig. 3. Chemical properties of MNF: (a) FT-IR spectra of MNF and its precursor materials, and (b) PXRD of MNF and its precursor material.

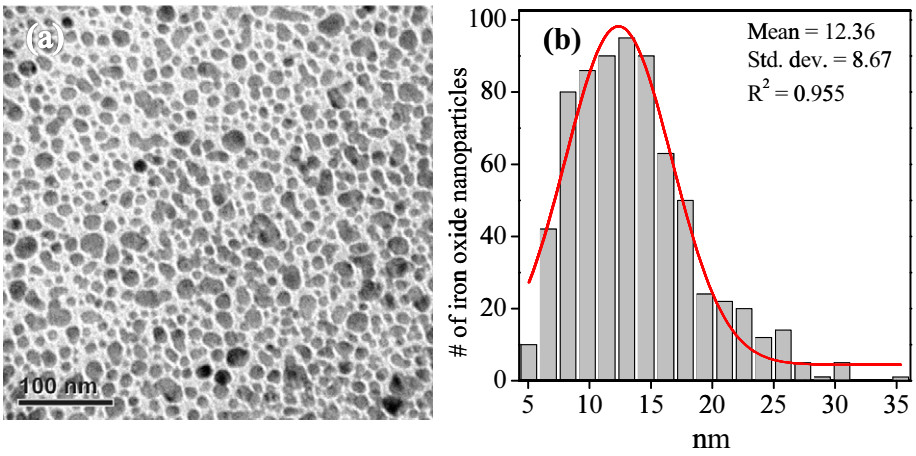

Fig. 4. Morphology of MNF: (a) TEM image and (b) the size range of iron oxide nanoparticles (IONs) (the total number of nanoparticles analyzed was 710).

the thermal decomposition also reflected the fraction of IONs in MNF, which was estimated to be 5%.

3.2. Decolorization in water using magnetic NOHMs fluid

Decolorization using MNF was demonstrated by removing Nile Blue dye from water. As a liquid material, it is critical to investigate the dissolution behavior of MNF in water prior to interacting with a target compound. Fig. 6(a) shows a glass vial filled with 2500 mg l^{-1} of MNF in water whose color is homogenous over the entire vial, revealing that MNF could be evenly suspended in water. Even though the concentration of MNF was increased to 10,000 mg l^{-1}, the color of solution still remained homogeneous (Fig. S4, see ESI†), demonstrating its high solubility in water owing to the hydrophilicity of polyetheramine. MNF can be collected via an external magnetic field as shown in Fig. 6(b) in which concentrated MNF can be seen on the left side of the vial where the magnet was placed. When Nile Blue dye was added to MNF solution (Fig. 6(c)), the color of the mixture readily became blackish blue (Nile Blue dye concentration was 50 mg l^{-1}). After the mixture was shaken for 2 h, the external magnet approached to the left side of the vial as shown in Fig. 6(d). It can be seen that MNF with Nile Blue dye can be separated from water. Fig. 7(a) depicts the removal capacity, q_t, of MNF as a function of the mixing time. It can be seen that the removal capacity rapidly increased from $t = 0$ to 20 min, followed by a series of gradual increments from $t = 20$ to 80 m, and reached equilibrium afterwards. This reveals that a longer mixing time could considerably improve the removal capacity of MNF. Yet there was a limit for this removal capacity possibly due to the limited reaction sites of IONs to interact with Nile Blue dye. Although MNF exhibited an apparent capability to decolorize Nile Blue dye in water, it may raise up a question that was the removal of Nile Blue dye by MNF simply because Nile Blue dye was adsorbed to the IONs? To clarify this, we also used IONs of a weight equivalent to the weight of IONs contained in MNF to decolorize Nile Blue in water. The removal capacity of the IONs was also shown in Fig. 7(a), which was significantly lower than the removal capacity of MNF. After 120-min mixing, MNF could reach 7.5 mg g^{-1} of removal capacity, whereas the IONs just exhibited 0.7 mg g^{-1}. Since the ION was located in the center of a unit of MNF and surrounded by the polymer chains, the ION in MNF might not fully expose to Nile Blue as the ION alone dispersed in water. Thus, the comparison suggested that the removal of Nile Blue dye by MNF could be mainly owing to the polymer chains of MNF. As shown in Fig. 1(a), each polyetheramine molecule consists of ~41 ether groups. It has been found that the fabrication of ether-containing polymers (e.g., polyethylene glycol and Triton X-100) on substrates could significantly enhance the adsorption of polar substrates, like cationic dyes, owing to the highly hydrophilic ethereal oxygen groups. Therefore, Nile Blue dye adsorption in MNF could be attributed to the presence of ether groups along each polyetheramine molecule [50,51]. Since MNF also consisted of hydroxyl and secondary amine groups which contained hydrogen atoms, MNF was also expected to interact with Nile Blue via the hydrogen bonding. The proposed mechanism for the dye adsorption was depicted in Fig. 8, in which

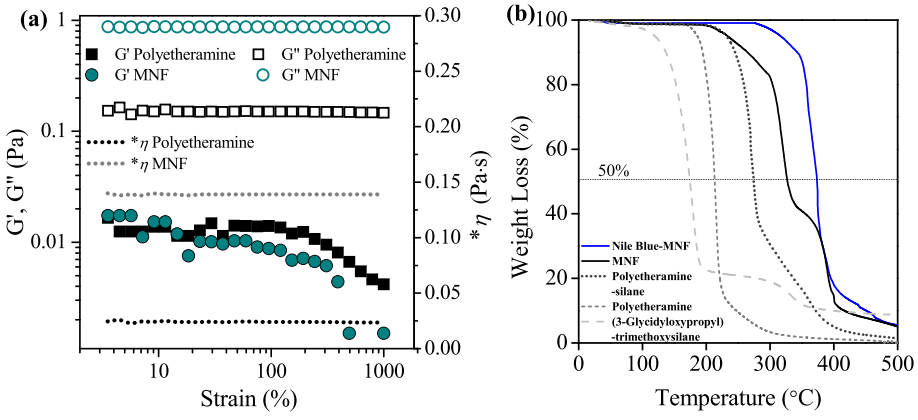

Fig. 5. Physical properties of magnetic NOHMs fluid (MNF) and its precursor materials: (a) storage and loss modules, and complex viscosities of MNF and PEA, (b) thermal stabilities of MNF, polyetheramine–silane, polyetheramine, (3-glycidyloxypropyl)-trimethoxysilane as well as Nile Blue-rich MNF.

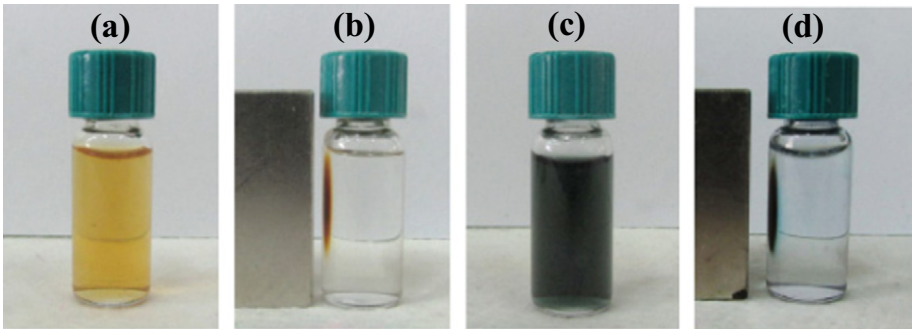

Fig. 6. Pictures of (a) dissolution of MNF in water (MNF aqueous solution, 2500 mg l^{-1}), (b) magnetic separation of MNF from water, (c) Nile Blue dye added to MNF aqueous solution (Nile Blue dye concentration was 50 mg l^{-1}) and (d) magnetic separation of Nile Blue-containing MNF from water.

Nile Blue can be attracted by MNF through the interaction between the ether group and quaternary amine as well as the hydrogen bonding between oxygen of Nile Blue and hydrogen along the MNF's polymer chains.

To further analyze the kinetic data of Nile Blue dye removed by MNF, we used the pseudo-first-order and the pseudo-second-order rate laws to examine the data. The pseudo-first-order equation:

$$q_t = q_e\left(1-e^{-k_1 t}\right) \tag{1}$$

where q_t and q_e are the removal capacity (mg g^{-1}) of MNF at the reaction time t (min) and at equilibrium, respectively. k_1 (min^{-1}) is the rate constant for the pseudo first order equation.

The pseudo-second-order equation:

$$q_t = \frac{k_2 q_e^2 t}{1 + k_2 q_e t} \tag{2}$$

where k_2 (g mg^{-1} min^{-1}) represents the rate constant for the pseudo second order equation. Fig. 7(b) shows that the kinetic data could be fitted using both rate laws. The fitting correlation coefficients were summarized in Table 1 which indicates the pseudo-second-order rate law ($R_2^2 = 0.998$) actually was a more satisfactory model than the pseudo-first-order rate law ($R_1^2 = 0.944$) to describe the kinetic data. Table 1 also lists the kinetic constants, k_1 and k_2, as well as the estimated removal capacity at equilibrium, $q_{e,est}$. It can be seen that the $q_{e,est}$ by the pseudo-second-order rate law was also closer to the experimental

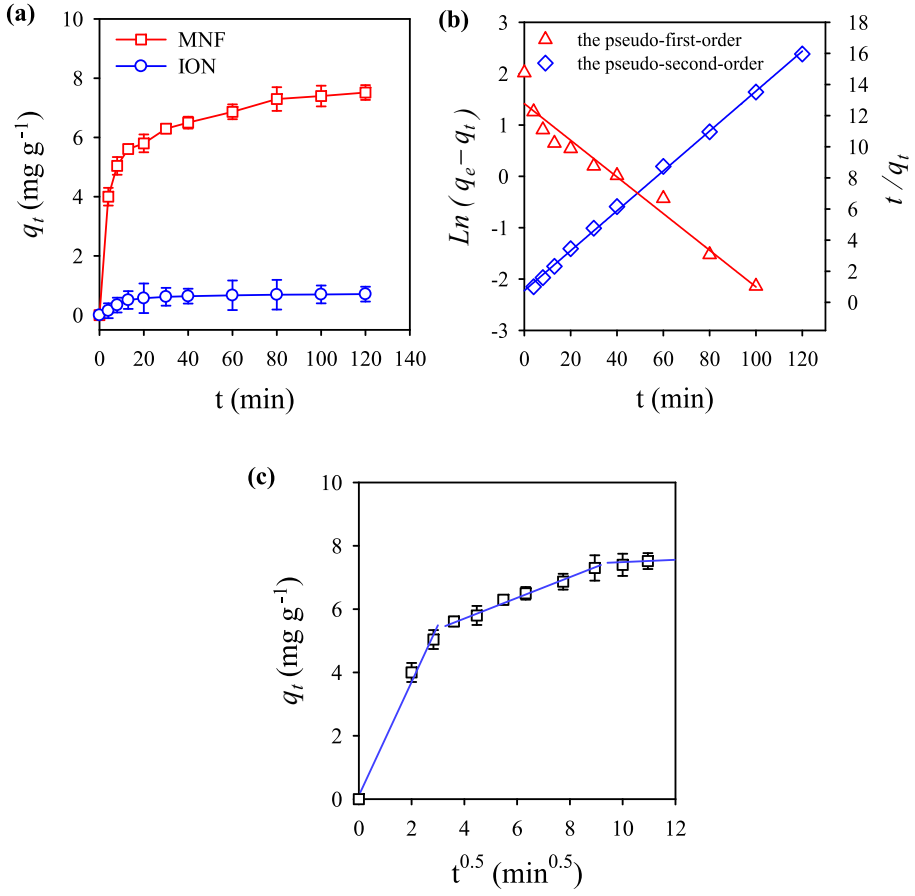

Fig. 7. Decolorization of Nile Blue dye ($C_0 = 50$ mg l^{-1}) in water using MNF ($m = 0.1$ g) at 25 °C: (a) removal capacity of MNF as a function of time, (b) the kinetic data analyzed using the pseudo first order and the pseudo second order equations and (c) the intra-particle diffusion modeling of the kinetic data.

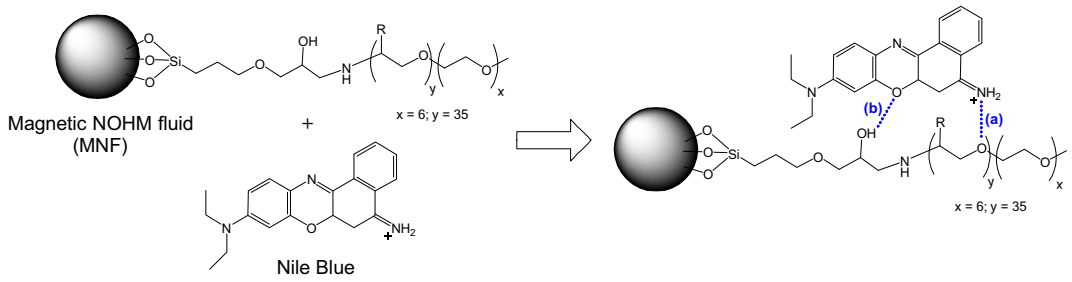

Fig. 8. Proposed scheme for the adsorption of Nile Blue to magnetic NOHMs fluid (MNF): (a) the interaction between the cationic quaternary amine and the ethereal oxygen group along the polymer chain and (b) hydrogen bonding between Nile Blue and the polymer chain of MNF.

removal capacity at equilibrium, $q_{e,exp}$, than the $q_{e,est}$ by the pseudo-first-order rate law. This also suggests that the pseudo-second-order was a more appropriate model to represent the kinetic data. However, these two models cannot provide information on diffusion of Nile Blue dye in water and in MNF. Therefore, the intra-particle diffusion model was also used to analyze the kinetic data as follows (Eq. (3)).

$$q_t = k_{P,i} t^{0.5} + C \tag{3}$$

where $k_{P,i}$ is the diffusion rate constant at different stage i and C represents the intercept which is associated with the thickness of the boundary layer [52]. Typically the adsorptive process proceeds in three stages: the first stage representing the external surface adsorption or the instant adsorption, so-called "boundary layer diffusion" [53], the second stage describing the gradual adsorption, and the third stage exhibiting the final equilibrium of the adsorption [54,55]. The intra-particle diffusion becomes a rate-limiting step during the second stage. However, the intra-particle diffusion process becomes slow during the third stage due to the decreasing remaining concentration of solutes [56].

Based on Eq. (3), a plot of q_t versus $t^{0.5}$ is shown in Fig. 7(c), which comprises three linear components representing the first, second, and third stages, respectively. The points were selected for each linear line, corresponding to each stage, based on the visual observation and examined by the linear regression to select the most appropriate points for each stage according to correlation coefficients. These three stages can be clearly distinguished, revealing that the removal of Nile Blue dye by MNF involved the boundary layer diffusion, the intra-particle diffusion and the adsorption equilibrium. All three linear components in Fig. 7(c) are quite close to straight lines which suggest that the intra-particle diffusion could be the dominant mechanism for the transfer of Nile Blue dye during the removal process [53]. The intra-particle diffusion rate constant, $k_{p,2}$, was also determined and listed in Table 1; the correlation coefficient (R_P^2) = 0.990, showing the linearity of the fitting line for the second stage.

3.3. Adsorption isotherm of dye from water

Since the decolorization of dye by MNF was considered as a result of the dye adsorption to MNF, it was important to investigate the decolorization behavior of MNF. Therefore, adsorption isotherm of Nile Blue dye by MNF was examined. In the adsorption isotherm experiment, the amount of MNF was fixed and various initial concentrations (40–160 mg l^{-1}) of Nile Blue dye in water were used. Fig. 9 shows a plot of C_e as a function of q_e. As the concentration gradient increased by raising up the initial concentration of Nile Blue dye, the removal capacity of MNF could be accordingly increased. However, the removal capacity seemingly reached a maximal value when the initial concentration reached a certain value. To model this adsorption behavior, the adsorption isotherm data were also analyzed using Langmuir, Freundlich, Temkin, and Dubinin–Radushkevich (D–R) isotherms as shown in Fig. S5 (see ESI†).

Langmuir isotherm represents one of the most widely-used models to describe the adsorption isotherm. The Langmuir model considers that adsorption is a mono-layer and occurs on a uniform surface where the number of adsorption sites is finite. Therefore, there is a maximal adsorption capacity which can be estimated by the Langmuir model. The linear form of the Langmuir model can be described in the following equation (Eq. (4)):

$$\frac{C_e}{q_e} = \frac{1}{K_L q_{\max}} + \frac{C_e}{q_{\max}} \tag{4}$$

where K_L represents the Langmuir constant and $q_{\max}$ represents the maximal dye removal capacity. A plot of C_e versus C_e/q_e is shown in Fig. S5(a) and the data points are fitted by the linear regression using Eq. (4). It can be seen that the data points were well-fitted by the regression line with a correlation coefficient of 0.981 (Table 2). This correlation coefficient suggests that Langmuir model could represent the adsorption isotherm data and the adsorption of Nile Blue to MNF could be mono-layer. This agrees with the decolorization mechanism discussed earlier that Nile Blue molecules were attracted to the specific sites along the polymer chain of MNF. Nile Blue molecules could be adsorbed and form the mono-layer on the polymer chain. The slope and intercept of the plot can be used to estimate $q_{\max}$ and K_L which were listed in Table 2. The $q_{\max}$ was found to be 38 mg g^{-1}. Up to date, a number of solid materials have been used to adsorb Nile Blue in water including alumina and acrylamide–maleic acid hydrogels. However, the adsorption capacities of these materials were relatively low (e.g., 4 mg g^{-1}) [57,58] compared to the estimated maximal adsorption capacity of MNF, showing that MNF in fact can be an efficient and promising material to remove Nile Blue from water. On the other hand, K_L was found to be 0.068 l mg^{-1}, showing that the adsorption-associated energy was relatively low.

Table 1
Model constants for decolorization by MNF derived from the pseudo-first-order, the pseudo-second-order equation and the intra-particle diffusion model.

$q_{e,exp}$ (mg g^{-1})	Pseudo-first-order			Pseudo-second-order				The intraparticle diffusion		
	k_1 (min^{-1})	$q_{e,fitted}$ (mg g^{-1})	R_1^2	k_2 (g mg−1 min^{-1})	$q_{e,fitted}$ (mg g^{-1})	h (mg g^{-1} min^{-1})	R_2^2	k_P (mg g^{-1} $min^{-0.5}$)	C	R_P^2
7.51	0.847	6.85	0.944	0.033	7.45	1.84	0.998	0.316	4.47	0.990

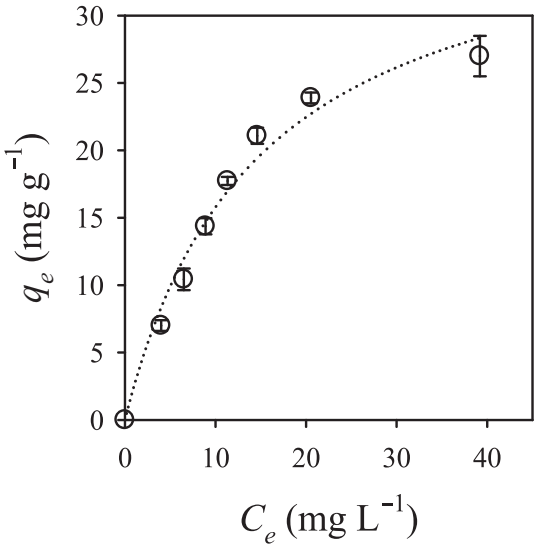

Fig. 9. Adsorption isotherm of Nile Blue dye to MNF at 25 °C (C_0 = 40–160 mg l^{-1} and weight of MNF = 0.1 g).

On the other hand, Fig. S5(b) shows the data points fitted by the Freundlich model which can be expressed in a linear form as follows (Eq. (5)):

$$\ln q_e = \ln K_F + \frac{1}{n} \ln C_e \tag{5}$$

where K_F is the Freundlich model constant and $1/n$ represents the heterogeneity factor of the sorbent. The Freundlich model assumes that mono-layer and multiple-layer adsorptions, representing chemisorption and physisorption, respectively, could occur during the adsorption process. Fig. S5(b) displays a plot of ln C_e versus ln q_e, in which the data points were not well fitted by the linear regression using the Eq. (5). The correlation coefficient was found to be only 0.914, indicating that the Freundlich was not a satisfactory model to describe the adsorption isotherm. This also suggests that the adsorption of Nile Blue did not involve both of chemisorption and physisorption together. The adsorption could be achieved just by chemisorption as discussed in the Langmuir model. However, the value of n was larger than 1, indicating that adsorption isotherm could be classified as L-type isotherm and a high affinity existed between MNF and Nile Blue [53].

In addition to the Langmuir and Freundlich models, we also examined another isotherm model associated with the chemisorption, Temkin isotherm. The Temkin model assumes that the adsorption energy diminishes correspondingly with the surface coverage in view of adsorbent–adsorbate interactions. Therefore, the Temkin model can be expressed as follows (Eq. (6)):

$$q_e = \frac{RT}{b} \ln K_T + \frac{RT}{b} \ln C_e \tag{6}$$

where b represents the Temkin model constant and K_T represents the Temkin isotherm constant. A plot of ln C_e versus q_e is shown in Fig. S5(c) and the data points were fitted by the linear regression using Eq. (6). Interestingly, the Temkin model seemed to be a satisfactory model for the isotherm data with a correlation coefficient of 0.970. This indicates that the adsorption of Nile Blue was associated with the available adsorption sites as a result of the chemisorption.

Since the Langmuir, Freundlich and Temkin isotherm models were related to the chemisorption, it was important to investigate whether the adsorption isotherm data could be represented by a physisorption-based isotherm. Thus, the Dubinin–Radushkevich (D–R) model was selected and used to examine the isotherm data. The D–R model assumes that adsorption process involves multiple layers and van der Waals forces. This model preferentially can be used for physisorption. The D–R model can be expressed as follows (Eq. (7)):

$$\ln q_e = \ln q_d - \beta\varepsilon^2 \tag{7}$$

where ε represents the Polanyi potential which can be calculated from $\varepsilon = RT\ln(1 + 1/C_e)$ and q_d is the theoretical isotherm saturation capacity. β represents the D–R isotherm constant. Fig. S5(d) shows a plot of ln q_e versus ε^2 which reveals that the D–R model was unsatisfactory to describe the isotherm data just with a correlation coefficient of 0.890. This suggests that the adsorption isotherm of Nile Blue to MNF was not based on the physisorption.

Based on the analysis of the adsorption isotherm using these four models, it can be deduced that the mechanism of adsorption of Nile Blue dye on MNF primarily involved the chemical interaction between the active sites of MNF (e.g., ether groups) and NB dye. This finding validated the proposed decolorization mechanism discussed in the earlier section. The affinity between Nile Blue molecules and the polymer chain of MNF led to the adsorption of Nile Blue to MNF.

3.4. Decolorization of other dyes in water using MNF

In this study, Nile Blue was selected as a model dye to investigate the performance and mechanism of the decolorization in water using MNF. We also examined whether MNF can decolorize other types of dyes in water, including malachite green, methylene blue, acid yellow 17 and acid red 27. The decolorization result (Fig. 10) shows that MNF could also decolorize these four dyes. However, the removal capacities of MNF for malachite green and methylene blue were much higher than those of acid yellow 17 and acid red 27. Since malachite green and methylene blue are cationic dyes, they could also be adsorbed to MNF based on the mechanism discussed in the earlier section owing to the ether–quaternary amine interaction. On the other hand, acid yellow 17 and acid red 27 were acidic dyes and therefore the affinity between MNF and these acid dyes was expected to be much less, resulting in the low removal capacities.

3.5. Physical and chemical properties of dye-containing magnetic NOHMs fluid

After MNF "captured" Nile Blue dye and was separated from water, this Nile Blue dye-containing MNF was dried to remove water content to exhibit dark blue color. To evaluate its fluidity and magnetic responsiveness, a drop of the Nile Blue dye-containing MNF was placed on top of a transparent lid as shown in Fig. 11. When a permanent magnet approached the Nile Blue dye-containing MNF, it started to flow and moved toward the magnet, showing that the Nile Blue dye-containing MNF still possessed the magnetic responsiveness and fluidity. On the other hand, we also tested the thermal stability of the Nile Blue dye-

Table 2
Adsorption isotherm model constants for decolorization by MNF derived from the Langmuir model, the Freundlich model, the Temkin and the Dubinin–Radushkevich isotherms.

Temp. (°C)	Langmuir			Freundlich			Temkin			Dubinin–Radushkevich		
	q_{max} (mg g^{-1})	K_L (l mg^{-1})	R_L^2	K_F (mg g^{-1}) (l mg^{-1})$^{1/n}$	n	R_F^2	K_T (l g^{-1})	b (J mol^{-1})	R_T^2	q_d (mg g^{-1})	$\beta \times 10^6$ (mol^2 kJ^{-1})	R_D^2
25	38.31	0.068	0.981	3.510	1.632	0.914	0.533	257.70	0.970	22.79	4.30	0.890

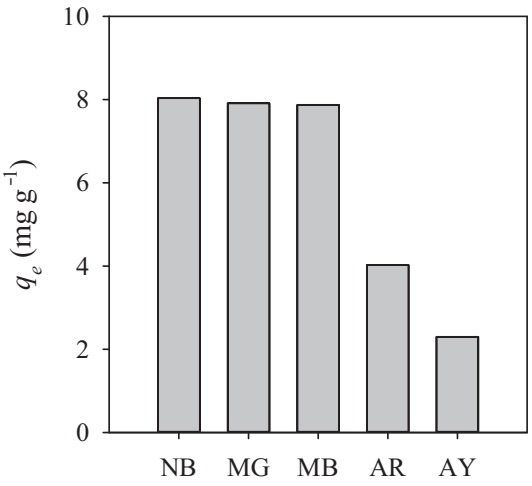

Fig. 10. Removal capacities of MNF for different dyes at 25 °C. NB: Nile Blue, MG: malachite green, MB: methylene blue, AR: acid red 27, AY: acid yellow 17. $C_0 = 50$ mg l^{-1}; weight of MNF = 0.1 g; the mixing time = 3 h.

containing MNF to investigate the effect of Nile Blue dye on the thermal stability of MNF. We have discussed the thermal stabilities of MNF and its precursor materials using Fig. 5(b) in the earlier section. The thermal stability of the Nile Blue dye-containing MNF can also be found in Fig. 5(b) as the blue TG curve which remained intact without any weight loss until 275 °C, revealing that Nile Blue dye-containing MNF exhibited an enhanced thermal stability compared to MNF. T_{50} for the Nile Blue dye-containing MNF was found to be 378 °C which was much higher than T_{50} of MNF. To clarify whether this enhancement in the Nile Blue dye-containing MNF was attributed to the presence of Nile Blue dye, the thermal stability of Nile Blue dye alone was also measured and shown in Fig. S6 (see ESI†). It can be seen that Nile Blue dye exhibited a superior thermal stability with T_{50} of 510 °C. Therefore, the enhanced thermal stability of the Nile Blue dye-containing MNF could be owing to the existence of Nile Blue dye adsorbed in MNF. This suggests that the recovered dye-containing MNF actually can be more thermally stable and therefore it can be used for other applications where a higher thermal stability is required.

4. Conclusion

In this study, we have successfully synthesized magnetic NOHMs fluid (MNF) with γ-Fe_2O_3 as cores and polyetheramine as polymer chains. MNF can exhibit magnetically controllable and responsive properties as well as liquid-like behaviors. In MNF, the IONs were found to mono-disperse in the polymer medium without apparent aggregation. Rheological measurements revealed that when polyetheramine was reacted with the IONs to form MNF, the viscosity of the composite was significantly higher than that of polyetheramine. However, MNF still could behave like a liquid. MNF also exhibited a greatly enhanced thermal stability which could be advantageous for MNF to be used in high-temperature applications. To examine MNF's applicability in aqueous solutions, the decolorization of dyes in water using MNF was demonstrated by removing Nile Blue dye from water. Therefore, this fluid and magnetically responsive MNF revealed the applicability of covalent-bonded NOHMs in aqueous solutions as well as a great potential as a magnetic solvent which can be used in other separation applications.

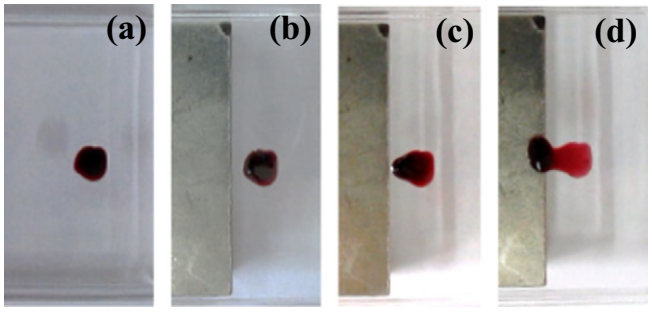

Fig. 11. Pictures (a)–(d) showing the response of Nile Blue-containing MNF under an external magnetic field.

Acknowledgment

K.-Y. A. Lin gratefully acknowledges the funding support (NSC 102-2218-E-005-003-) from the Ministry of Science and Technology, R.O.C. The authors thank Prof. Wenjea Tseng and Dr. Chir-Jang Tsai in the Department of Materials Science and Engineering at NCHU for their assistance on the rheological measurement. The authors also thank Mr. Andrew P. Jochems for his suggestions on the English writing.

Appendix A. Supplementary data

Supplementary data to this article can be found online at http://dx.doi.org/10.1016/j.molliq.2015.01.020.

References

[1] A.B. Bourlinos, S.R. Chowdhury, R. Herrera, N. Chalkias, D.D. Jiang, Q. Zhang, L.A. Archer, E.P. Giannelis, Functionalized nanostructures with liquid-like behavior: expanding the gallery of available nanostructures, Adv. Funct. Mater. 15 (2005) 1285–1290.
[2] A.B. Bourlinos, R. Herrera, N. Chalkias, D.D. Jiang, Q. Zhang, L.A. Archer, E.P. Giannelis, Surface-functionalized nanoparticles with liquid-like behavior, Adv. Mater. 17 (2005).
[3] K.-Y.A. Lin, A.-H.A. Park, Effects of bonding types and functional groups on CO_2 capture using novel multiphase systems of liquid-like nanoparticle organic hybrid materials, Environ. Sci. Technol. 45 (15) (2011) 6633–6639.
[4] Y. Park, J. Decatur, K.-Y.A. Lin, A.-H.A. Park, Investigation of CO_2 capture mechanisms of liquid-like nanoparticle organic hybrid materials via structural characterization, Phys. Chem. Chem. Phys. (2011). http://dx.doi.org/10.1039/c1cp22631b.
[5] C. Petit, Y. Park, K.-Y.A. Lin, A.-H.A. Park, Spectroscopic investigation of the canopy configurations in nanoparticle organic hybrid materials of various grafting densities during CO_2 capture, J. Phys. Chem. C 116 (2011) 516–525.
[6] C. Petit, S. Bhatnagar, A.-H.A. Park, Effect of water on the physical properties and carbon dioxide capture capacities of liquid-like nanoparticle organic hybrid materials and their corresponding polymers, J. Colloid Interface Sci. 407 (2013) 102–108.
[7] R. Rodriguez, R. Herrera, A.B. Bourlinos, R. Li, A. Amassian, L.A. Archer, E.P. Giannelis, The synthesis and properties of nanoscale ionic materials, Appl. Organomet. Chem. 24 (2010) 581–589.
[8] R. Rodriguez, R. Herrera, L.A. Archer, E.P. Giannelis, Nanoscale ionic materials, Adv. Mater. 20 (2008) 4353–4358.
[9] J. Texter, Interfaces in advanced materials, Curr. Opin. Colloid Interface Sci. 19 (2014) 43–48.
[10] L. Wu, B. Zhang, H. Lu, C.-Y. Liu, Nanoscale ionic materials based on hydroxyl-functionalized graphene, J. Mater. Chem. A 2 (2014) 1409–1417.
[11] P. Agarwal, L.A. Archer, Strain-accelerated dynamics of soft colloidal glasses, Phys. Rev. E. 83 (2011) 041402.
[12] P. Agarwal, H. Qi, L.A. Archer, The ages in a self-suspended nanoparticle liquid, Nano Lett. 10 (2009) 111–115.
[13] C. Petit, K.-Y.A. Lin, A.-H.A. Park, Design and characterization of liquid-like POSS-based hybrid nanomaterials synthesized via ionic bonding and their interactions with CO_2, Langmuir 29 (39) (2013) 12234–12242.
[14] A.B. Bourlinos, A. Bakandritsos, V. Georgakilas, V. Tzitzios, D. Petridis, Facile synthesis of capped γ-Fe_2O_3 and Fe_3O_4 nanoparticles, J. Mater. Sci. 41 (2006) 5250–5256.
[15] A.B. Bourlinos, A. Stassinopoulos, D. Anglos, R. Herrera, S.H. Anastasiadis, D. Petridis, E.P. Giannelis, Functionalized ZnO nanoparticles with liquidlike behavior and their photoluminescence properties, Small 2 (2006) 513–516.
[16] Q. Li, L. Dong, J. Fang, C. Xiong, Property–structure relationship of nanoscale ionic materials based on multiwalled carbon nanotubes, ACS Nano 4 (2010) 5797–5806.
[17] D. Kim, L.A. Archer, Nanoscale organic–inorganic hybrid lubricants, Langmuir 27 (2011) 3083–3094.
[18] J.L. Nugent, S.S. Moganty, L.A. Archer, Nanoscale organic hybrid electrolytes, Adv. Mater. 22 (2010) 3677–3680.
[19] S.S. Moganty, N. Jayaprakash, J.L. Nugent, J. Shen, L.A. Archer, Ionic-liquid-tethered nanoparticles: hybrid electrolytes, Angew. Chem. 122 (2010) 9344–9347.
[20] H. Wang, K.-Y. Lin, B. Jing, G. Krylova, G.E. Sigmon, P. McGinn, Y. Zhu, C. Na, Removal of oil droplets from contaminated water using magnetic carbon nanotubes, Water Res. 47 (2013) 4198–4205.

[21] K.-Y.A. Lin, A.-H.A. Park, Effects of bonding types and functional groups on CO_2 capture using novel multiphase systems of liquid-like nanoparticle organic hybrid materials, Environ. Sci. Technol. 45 (2011) 6633–6639.
[22] P.K. Malik, Dye removal from wastewater using activated carbon developed from sawdust: adsorption equilibrium and kinetics, J. Hazard. Mater. 113 (2004) 81–88.
[23] J.-L. Gong, B. Wang, G.-M. Zeng, C.-P. Yang, C.-G. Niu, Q.-Y. Niu, W.-J. Zhou, Y. Liang, Removal of cationic dyes from aqueous solution using magnetic multi-wall carbon nanotube nanocomposite as adsorbent, J. Hazard. Mater. 164 (2009) 1517–1522.
[24] H. Sun, L. Cao, L. Lu, Magnetite/reduced graphene oxide nanocomposites: one step solvothermal synthesis and use as a novel platform for removal of dye pollutants, Nano Res. 4 (2011) 550–562.
[25] Y. Dong, B. Lu, S. Zang, J. Zhao, X. Wang, Q. Cai, Removal of methylene blue from coloured effluents by adsorption onto SBA-15, J. Chem. Technol. Biotechnol. 86 (2011) 616–619.
[26] D.D. Asouhidou, K.S. Triantafyllidis, N.K. Lazaridis, K.A. Matis, S.-S. Kim, T.J. Pinnavaia, Sorption of reactive dyes from aqueous solutions by ordered hexagonal and disordered mesoporous carbons, Microporous Mesoporous Mater. 117 (2009) 257–267.
[27] G. Bayramoglu, B. Altintas, M.Y. Arica, Adsorption kinetics and thermodynamic parameters of cationic dyes from aqueous solutions by using a new strong cation-exchange resin, Chem. Eng. J. 152 (2009) 339–346.
[28] M.P. Pileni, Magnetic fluids: fabrication, magnetic properties, and organization of nanocrystals, Adv. Funct. Mater. 11 (2001) 323–336.
[29] M. Zahn, Magnetic fluid and nanoparticle applications to nanotechnology, J. Nanoparticle Res. 3 (2001) 73–78.
[30] R.E. Rosensweig, R. Kaiser, G. Miskolczy, Viscosity of magnetic fluid in a magnetic field, J. Colloid Interface Sci. 29 (1969) 680–686.
[31] N. Moumen, M.P. Pileni, Control of the size of cobalt ferrite magnetic fluid, J. Phys. Chem. 100 (1996) 1867–1873.
[32] M. Saleem, M. Afzal, F. Mahmood, A. Hameed, Thermodynamics of adsorption of rhodamin B and Nile blue sulfate on alumina from aqueous solutions, J. Chem. Soc. Pak. 16 (1994) 83–86.
[33] H. Miao, J. Li, Y. Lin, X. Liu, Q. Zhang, J. Fu, Characterization of γ-Fe_2O_3 nanoparticles prepared by transformation of α-FeOOH, Chin. Sci. Bull. 56 (2011) 2383–2388.
[34] T. Theppaleak, G. Tumcharern, U. Wichai, M. Rutnakornpituk, Synthesis of water dispersible magnetite nanoparticles in the presence of hydrophilic polymers, Polym. Bull. 63 (2009) 79–90.
[35] Y. Zhang, G.K. Das, R. Xu, T.T. Yang Tan, Tb-doped iron oxide: bifunctional fluorescent and magnetic nanocrystals, J. Mater. Chem. 19 (2009) 3696–3703.
[36] N. Wang, Q. Fang, E. Chen, J. Zhang, Y. Shao, Structure, crystallization behavior, and thermal stability of PP/MCM-41 nanocomposite, Polym. Eng. Sci. 49 (2009) 2459–2466.
[37] V. Mittal, Thermal characterization of fillers and polymer nanocomposites, Characterization Techniques for Polymer Nanocomposites, Wiley-VCH Verlag GmbH & Co. KGaA, 2012, pp. 13–32.
[38] P. Liu, Z. Su, Thermal stabilities of polystyrene/silica hybrid nanocomposites via microwave-assisted in situ polymerization, Mater. Chem. Phys. 94 (2005) 412–416.
[39] H. Sugimoto, K. Daimatsu, E. Nakanishi, Y. Ogasawara, T. Yasumura, K. Inomata, Preparation and properties of poly(methylmethacrylate)–silica hybrid materials incorporating reactive silica nanoparticles, Polymer 47 (2006) 3754–3759.
[40] J.W. Gilman, Flammability and thermal stability studies of polymer layered-silicate (clay) nanocomposites, Appl. Clay Sci. 15 (1999) 31–49.
[41] J.W. Gilman, C.L. Jackson, A.B. Morgan, R. Harris, E. Manias, E.P. Giannelis, M. Wuthenow, D. Hilton, S.H. Phillips, Flammability properties of polymer-layered-silicate nanocomposites. Polypropylene and polystyrene nanocomposites†, Chem. Mater. 12 (2000) 1866–1873.
[42] Z. Peng, L.X. Kong, A thermal degradation mechanism of polyvinyl alcohol/silica nanocomposites, Polym. Degrad. Stab. 92 (2007) 1061–1071.
[43] Z. Peng, L.X. Kong, S.-D. Li, Thermal properties and morphology of a poly(vinyl alcohol)/silica nanocomposite prepared with a self-assembled monolayer technique, J. Appl. Polym. Sci. 96 (2005) 1436–1442.
[44] D.M. Marquis, E. Guillaume, C. Chivas-Joly, Nanocomposites and Polymers With Analytical Methods, Intech, 2011.
[45] E.P. Giannelis, Polymer Layered Silicate Nanocomposites, Adv. Mater. 8 (1996) 29–35.
[46] S. Pavlidou, C.D. Papaspyrides, A review on polymer-layered silicate nanocomposites, Prog. Polym. Sci. 33 (2008) 1119–1198.
[47] L.A. Utracki, Clay-containing Polymeric Nanocomposites, Rapra, Shawbury, 2004.
[48] M. Zanetti, P. Bracco, L. Costa, Thermal degradation behaviour of PE/clay nanocomposites, Polym. Degrad. Stab. 85 (2004) 657–665.
[49] J. Zhu, A.B. Morgan, F.J. Lamelas, C.A. Wilkie, Fire properties of polystyrene–clay nanocomposites, Chem. Mater. 13 (2001) 3774–3780.
[50] S.K. Parida, B.K. Mishra, Adsorption of styryl pyridinium dyes on polyethylene–glycol-treated silica, Colloids Surf. A Physicochem. Eng. Asp. 134 (1998) 249–255.
[51] K. Mishra, A.K. Sahay, B.K. Mishra, Behaviour of surface active cyanine dyes in water and surfactant solutions, Indian J. Chem. A 30 (1991) 886–889.
[52] F.-C. Wu, R.-L. Tseng, R.-S. Juang, Kinetic modeling of liquid-phase adsorption of reactive dyes and metal ions on chitosan, Water Res. 35 (2001) 613–618.
[53] W.H. Cheung, Y.S. Szeto, G. McKay, Intraparticle diffusion processes during acid dye adsorption onto chitosan, Bioresour. Technol. 98 (2007) 2897–2904.
[54] R. Han, P. Han, Z. Cai, Z. Zhao, M. Tang, Kinetics and isotherms of Neutral Red adsorption on peanut husk, J. Environ. Sci. 20 (2008) 1035–1041.
[55] X. Yu, G. Zhang, C. Xie, Y. Yu, T. Cheng, Q. Zhou, Equilibrium, kinetic, and thermodynamic studies of hazardous dye Neutral Red biosorption by spent corncob substrate, Bioresources 6 (2011) 936–949.
[56] P. Luo, Y. Zhao, B. Zhang, J. Liu, Y. Yang, J. Liu, Study on the adsorption of Neutral Red from aqueous solution onto halloysite nanotubes, Water Res. 44 (2010) 1489–1497.
[57] D. Saraydin, E. Karadağ, O. Güven, Adsorption of some basic dyes by acrylamide–maleic acid hydrogels, Sep. Sci. Technol. 31 (1996) 423–434.
[58] M. Saleem, M. Afzal, F. Mahmood, A. Hameed, Thermodynamics of adsorption of Rhodamine B and Nile blue sulphate on alumina from aqueous solutions, J. Chem. Soc. Pak. 16 (1994) 83–86.